Risk assessment of contrail formation using AIRS, MOZAIC and AERO2k databases

N. Lamquin* , C.J. Stubenrauch, S. Cros
Laboratoire de Météorologie Dynamique, Ecole Polytechnique, CNRS/IPSL, Palaiseau, France

H. Smit
Forschungzentrum Jülich, Institut für Chemie der belasteten Atmosphäre (ICG2), Jülich, Germany

Keywords: potential contrail occurrence, satellite observations

ABSTRACT: Ice supersaturation is a condition for contrails to persist and to induce additional cloud coverage. We use 6 years of the Atmospheric InfraRed Sounder (AIRS) data to determine the frequency of occurrence of potential persistent contrails over the globe. Since the relative humidity is retrieved over atmospheric layers of about 2 km depth, we use collocated data from the Measurements of OZone and water vapour by in-service AIrbus airCraft experiment (MOZAIC) to develop a correction algorithm for a better estimation of the frequency of ice supersaturation using the AIRS data. In addition, the AIRS cloud properties, retrieved at Laboratoire de Météorologie Dynamique (LMD), help to determine the occurrence of situations where persistent contrails would have the highest radiative impact. The AERO2k database, a global monthly inventory of aircraft traffic for the year 2002, is used to provide insight of the role played by the air traffic density.

1 INTRODUCTION

Condensation trails from aircrafts have a potential impact on the Earth's radiation budget by forming ice clouds in the upper troposphere. Ice supersaturation is a condition for contrails to persist and to induce additional high cloud coverage. We use atmospheric profiles of specific humidity and temperature from AIRS L2 data to determine relative humidity RHi_a over pressure layers with a depth of 50 or 100 hPa (corresponding to about 2 km) in the upper troposphere. Since humidity can only be determined as an integrated property over an atmospheric layer from IR sounders, where the depth of the layers depends on the spectral resolution of the instrument, this prevents the detection of ice supersaturated portions shallower than the vertical resolution. By collocating the AIRS relative humidity profiles with measurements from the MOZAIC experiment, the latter were taken at specific flight levels, we were able to develop a correction algorithm for a better estimation of the frequency of ice supersaturation when using the AIRS data. This algorithm determines the probability of ice supersaturation occurrence within a given AIRS profile, even when the integrated relative humidity determined by AIRS is lower than saturation (100%). The AIRS-LMD cloud property retrieval (Stubenrauch et al., 2008, 2009) helps to identify situations where persistent contrails would have the highest radiative impact (over clear and mostly clear situations). Frequency of occurrence of these situations is determined over the AIRS pressure layers in the upper troposphere. The AERO2k database, a global monthly inventory of aircraft traffic for the year 2002, is used to integrate these frequencies by means of the density of the global air traffic. It identifies regions and seasons with highest risk of persistent contrail formation, where the impact on climate is the largest.

2 DATA HANDLING

Since May 2002 the AIRS instrument (Chahine et al., 2006) onboard the polar orbiting satellite Aqua provides very high spectral resolution measurements of Earth emitted radiation in three spectral bands (3.74-4.61 micron, 6.20-8.22 micron and 8.80-15.40 micron) from 2378 channels, at 1:30

* *Corresponding author:* Nikolas Lamquin, Laboratoire de Météorologie Dynamique CNRS/IPSL CNRS/IPSL LMD Ecole Polytechnique 91128 Palaiseau France Email: nicolas.lamquin@gmail.com

and 13:30 local time. The spatial resolution of these measurements is 13.5 km at nadir. Nine AIRS measurements (3x3) correspond to one footprint of the Advanced Microwave Sounder Unit (AMSU). AIRS L2 standard products include temperature at 28 pressure levels from 0.1 hPa to the surface and water vapour mixing ratios in 14 pressure layers from 50 hPa to the surface (Susskind et al., 2003, 2006). These atmospheric profiles were retrieved from cloud-cleared AIRS radiances (Chahine et al., 2006) within each AMSU footprint, at a spatial resolution of about 45 km. We use version 5 of AIRS L2 data and retrieve relative humidity RHi_a in five pressure layers, 150-200, 200-250, 250-300, 300-400, and 400-500 hPa, as in Lamquin et al., 2009. Cloud properties (pressure and effective emissivity) have been retrieved at LMD and evaluated with CALIPSO data (Stubenrauch et al., 2008, 2009). This cloud climatology covers the whole globe over a period from 2003 - 2008 and also allows a distinction between clear and cloudy situations. This enables us to consider climatological situations nesting potential contrails where they have the highest radiative impact (over mostly clear areas).

The MOZAIC experiment (Marenco et al., 1998) gathered temperature, pressure and water vapor from commercial airplanes measurements over the period August 1994 - December 2007. Compared to the relative humidity determined from AIRS over pressure layers, these measurements were taken at specific levels (at flight altitudes). For detecting ice supersaturation in the upper troposphere we will use relative humidity over ice RHi_m as derived in Gierens et al. (1999). We have collocated these data with the AIRS data to determine a correction algorithm for the detection of ice supersaturation within the AIRS data. The implementation of this algorithm gives a better estimation of the occurrence of ice supersaturation and therefore of potential persistent contrails. The EU Fifth Framework Programme project AERO2k (Eyers et al., 2004) provides a global monthly inventory of flown distance for civil and military aircrafts in a 1° latitude x 1° longitude grid and with a vertical resolution of 500 feet (about 150 m) for the year 2002. From these data we have determined the air traffic density within the AIRS pressure layers over which our analyses are made.

3 AIRS-MOZAIC SYNERGY FOR A BETTER ESTIMATION OF THE FREQUENCY OF OCCURRENCE OF ICE SUPERSATURATION

Kahn et al. (2008) and Lamquin et al. (2008) have shown that the AIRS vertical resolution limits the estimation of ice supersaturation occurrence within a pressure layer. Lamquin et al. (2009) suggest a s-shaped probability function of the occurrence of ice supersaturation within an atmospheric pressure layer as function of the relative humidity averaged over the whole layer (in this case RHi_a). Such an s-function is certainly dependent on the vertical resolution. The collocation of ice supersaturation detected by MOZAIC at a certain level with the relative humidity determined from AIRS over a pressure layer permits to build such a function. We introduce uncertainties based on the MOZAIC uncertainties of +/- 10% and the relationship found (Fig.1) is shown for occurrences of RHi_m higher than 90, 100 or 110% (Fig. 1).

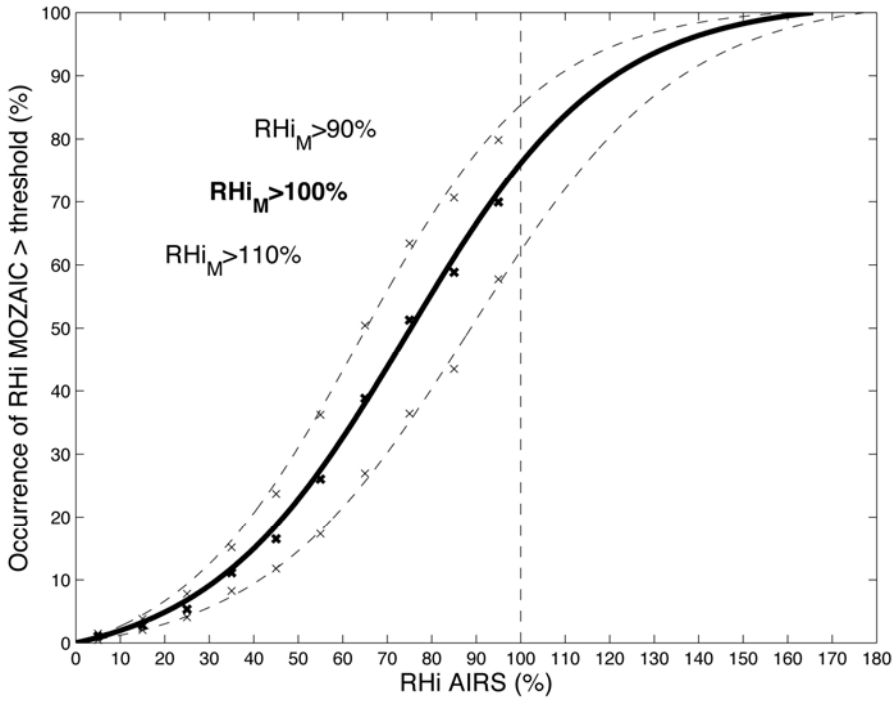

Figure 1: S-shaped functions of the probability of occurrence of ice supersaturation detected by MOZAIC as a function of the relative humidity determined from AIRS. Thresholds for the detection of ice supersaturation are 90%, 100%, or 110 %.

We observe the following: 1) a significant probability of occurrence of ice supersaturation within the AIRS pressure layer is found even when RHi_a is smaller than 100%. This is expected as Kahn et al. (2008) and Lamquin et al. (2008) have already shown that very shallow ice clouds are concomitant with low RHi_a. 2) the occurrence of ice supersaturation found by MOZAIC is only about 75% for RHi_a values around saturation. This can first be explained by the fact that the MOZAIC flight level does not always coincide with the altitude of the ice supersaturation layer within the AIRS pressure layer. In addition, there can be an effect of the uncertainties related to the determination of the relative humidity within the AIRS data. Lamquin et al. (2009) show that this uncertainty can reach 30% for RHi_a around saturation.

The s-function is then applied to the AIRS data in order to estimate the ice supersaturation occurrence over each AIRS pressure layer between 150 and 500 hPa. A weighting by the average flight altitude from the AERO2k database provides an integrated view of ice supersaturation occurrence at air traffic flight altitude (here over clear and partly cloudy situations, Fig.2). The map compares well to the results of Gierens et al. (2000) and extends their result to the whole globe.

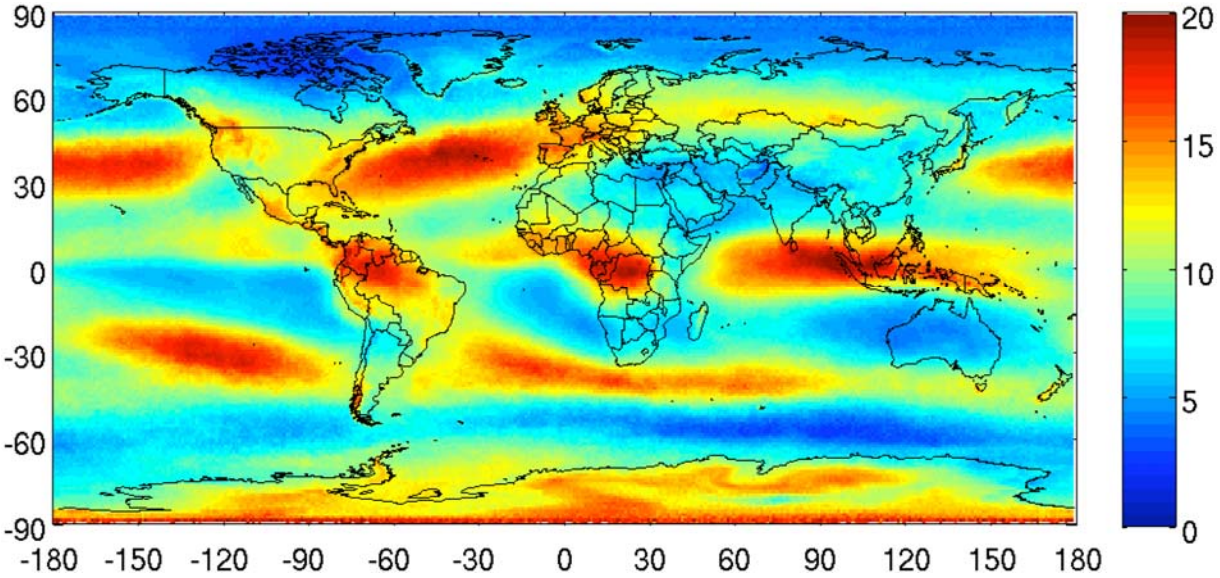

Figure 2: Global frequency of occurrence of ice supersaturation for clear and partly cloudy situations over the years 2003-2008 and integrated by the mean flight altitude in the upper troposphere.

4 RISK ASSESSMENT OF CONTRAIL FORMATION

Persistent contrails have the largest radiative effect over clear skies or situations with a low cloud amount (Stuber and Forster, 2007). It is possible to establish a separation between low and high cloudiness using the AIRS cloud properties. This, in addition to the Schmidt-Appleman criterion for the formation of contrails (Schumann, 1996), leads to a global climatology of the frequency of occurrence of persistent potential contrails as proposed, for example, in Sausen et al. (1998). Again, the results (Fig.3) are produced over AIRS pressure layers and the average flight altitude provides an integrated view of the global potential persistent contrail frequency of occurrence. The results compare well to Sausen et al. (1998).

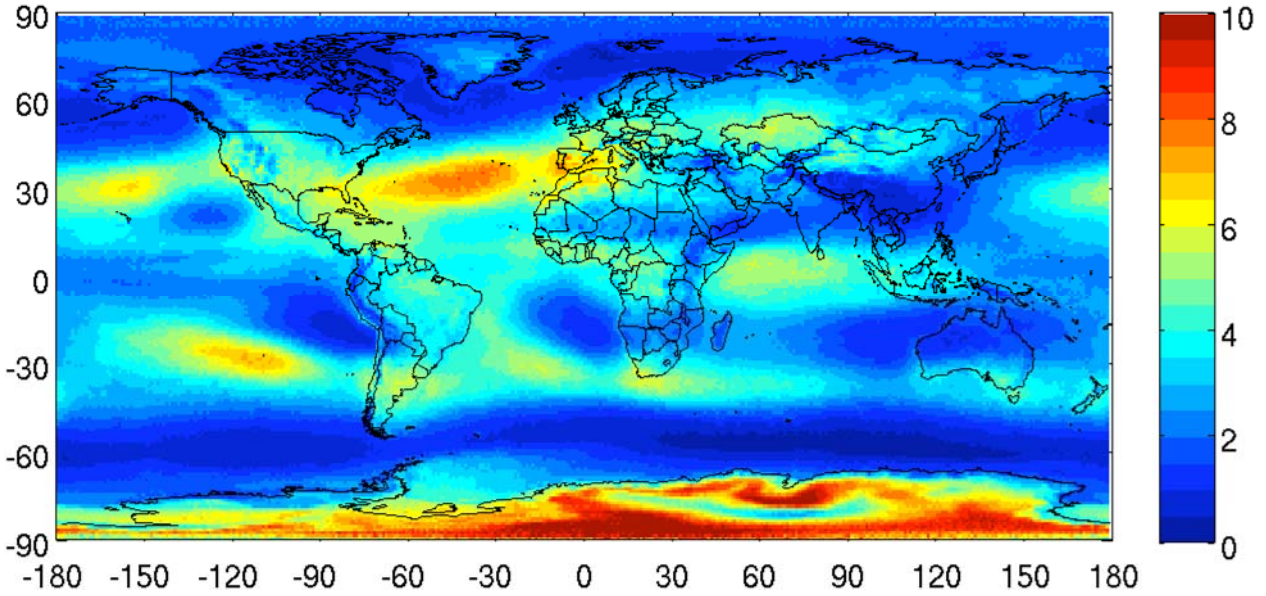

Figure 3: Global frequency of occurrence of potential persistent contrails having an impact on climate over the years 2003-2008 and integrated by the mean flight altitude in the upper troposphere.

Now, the AERO2k database not only provides vertical density of the air traffic. The distance flown by aircrafts forming contrails is proportional to the additional cloud coverage induced by contrails (Gierens, 1998). Accounting for the whole (horizontal and vertical) air traffic density, along with the climatological risk of formation, persistence and impact of contrails, provides a comparison between the total air traffic in the upper troposphere and the total air traffic in the upper troposphere producing contrails.

Both results (Fig.4) are normalized by the highest value over the globe. We see that the North-Atlantic Flight Corridor (NAFC) exhibits a second branch of comparable risk of formation of persistent contrails having an impact on climate. This effect is induced by the much higher potential contrail frequency of occurrence despite the lower air traffic density in the southern region of the NAFC.

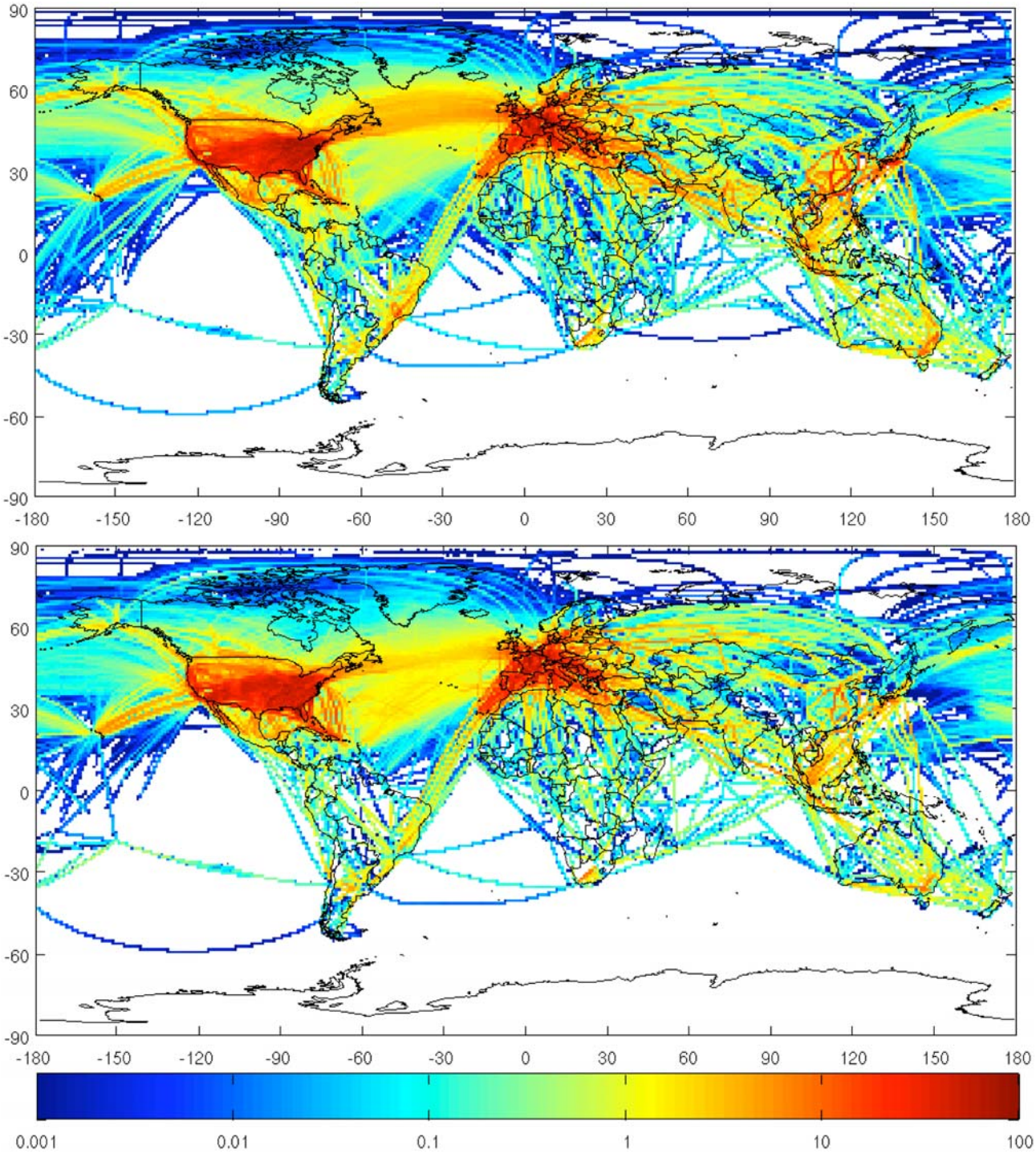

Figure 4: Density of air traffic in the upper troposphere (top) and density of potential persistent contrails having an impact on climate (bottom).

5 CONCLUSIONS

The synergy of ice supersaturation detection from MOZAIC and relative humidity profiles from AIRS was used to build a correction algorithm for a better determination of occurrence of ice supersaturation in the upper troposphere. Ice supersaturation occurrence over pressure layers in the upper troposphere is determined by AIRS over the whole globe over 6 years and expands regional MOZAIC results.

The combination with the AIRS-LMD cloud properties and the application of the Schmidt-Appleman criterion on AIRS relative humidity provides a climatology of the risk of formation, persistence and impact on climate of contrails. Occurrence of potential contrails has been determined

for situations with largest impact (zonal means of about 5% ±2%). There exists a rough agreement with analyses using ECMWF reanalyses, but AIRS provides more detailed horizontal structures.
Weighted by air traffic density, provided by the AERO2k database, one result shows that the NAFC exhibits two branches of the air traffic with comparable risk of contrail impact on climate despite the lower air traffic density in the southern branch.
In the future we will consider comparisons with observations of contrails (Vazquez-Navarro et al., 2009) and more recent climatologies of ice supersaturation and potential contrails from models (Burkhardt et al., 2008) and radiosoundings (Dickson et al., 2009).

REFERENCES

Burkhardt, U., B. Kärcher, M. Ponater, K. Gierens, and A. gettelman, 2008 : Contrail cirrus supporting areas. *Geophys. Res. Lett. 35*, L16808, doi :10.1029/2008GL034056.

Dickson, N., K. Gierens, H. Rogers, and R. Jones, 2009 : Vertical spatial scales of ice supersaturation. *This conference proceedings*.

Chahine, M.T., and Coauthors, 2006 : AIRS : Improving weather forecasting and providing new data on greenhouse gases. *Bull. Amer. Meteor. Soc. 87*, 911-926.

Eyers, C.J., P. Norman, J. Middel, M. Plohr, K. Atkinson, and R.A. Christou, 2004 :AERO2k global aviation emission inventories for 2002 and 2025. QinetiQ Ltd. Retrieved from http://www.aero-net.org/pdf-docs/AERO2K_Global_Aviation_Emissions_Inventories_for_2002_and_2025.pdf.

Gierens, K., 1998 : How the sky gets covered with contrails. *Meteorol. Z. 7*, 181-187.

Gierens, K., U. Schumann, M. Helten, H.G.J. Smit, and A. Marenco, 1999 : A distribution law for relative humidity in the upper troposphere and lower stratosphere derived from three years of MOZAIC measurements. *Ann. Geophys. 17*, 1218-1226.

Gierens, K., U. Schumann, M. Helten, H. Smit, and P.-H. Wang, 2000 : Ice-supersaturated regions and subvisible cirrus in the northern midlatitudes upper troposphere. *J. Geophys. Res. 105*, D18, 22743-22753.

Kahn, B.H., C.K. Liang, A. Eldering, A. Gettelman, Q. Yue, and K.N. Liou, 2008 : Tropical thin cirrus and relative humidity observed by the Atmospheric Infrared Sounder. *Atmos. Chem. Phys. 8*, 1501-1518.

Lamquin, N., C.J. Stubenrauch, and J. Pelon, 2008 : Upper tropospheric humidity and cirrus geometrical and optical thickness : relationships inferred from one year of collocated AIRS-CALIPSO data. *J. Geophys. Res. 113*, D00A08, doi :10.1029/2008JD010012.

Lamquin, N., K. Gierens, C.J. Stubenrauch, and R. Chaterjee, 2009 : Evaluation of upper tropospheric humidity forecasts from ECMWF using AIRS and CALIPSO data.. *Atmos. Chem. Phys. 9*, 1779-1793.

Marenco, A., V. Thouret, P. Nédélec, H.G. Smit, M. Helten, D. Kley, F. Karcher, P. Simon, K. Law, J. Pyle, G. Poschmann, R. Von Wrede, C. Hume, and T. Cook, 1998 : Measurements of ozone and water vapour by in-service Airbus aircraft : the MOZAIC airborne program, an overview. *J. Geophys. Res. 103*, 25631-25642.

Sausen, R., K. Gierens, M. Ponater, and U. Schumann, 1998 : A diagnostic study of the global distributions of contrails part I : present day climate. *Theor. Appl. Climatol. 61*, 127-141.

Schumann, U., 1996 : On conditions for contrail formation from aircraft exhausts. *Meteorol. Z. 5*, 4-23.

Stubenrauch, C.J., S. Cros, N. Lamquin, R. Armante, A. Chédin, C. Crevoisier, and N.A. Scott, 2008 : Cloud properties from AIRS and evaluation with CALIPSO. *J. Geophys. Res. 113*, D00A10, doi :10.1029/2008JD009928.

Stubenrauch, C.J., S. Cros, A. Guignard, and N. Lamquin, 2009 : A 6-year global climatology from the Atmospheric InfraRed Sounder aboard the Aqua satellite : statistical analysis in synergy with CALIPSO and Cloudsat. *In prep.*

Stuber, N., and P. Forster, 2007 : The impact of diurnal variations of air traffic on contrail radiative forcing. *Atmos. Chem. Phys. 7*, 3151-3162.

Susskind, J., C. Barnet, and J. Blaisdell, 2003 : Retrieval of atmospheric and surface parameters from AIRS/AMSU/HSB data in the presence of clouds. *IEEE Trans. Geosci. Remote Sens. 41*, 390-409.

Susskind, J., C. Barnet, J. Blaisdell, L. Iredell, F. Keita, L. Kouvaris, G. Molnar, and M. Chahine, 2006 : Accuracy of geophysical parameters derived from AIRS/AMSU as a function of fractional cloud cover. *J. Geophys. Res. 111*, D09S17, doi :10.1029/2005JD006272.

Vazquez-Navarro, M., H. Mannstein, and B. Mayer, 2009 : Lifecycle of contrails. *This conference proceedings.*

Aviation emissions under climate stabilization at 450ppmv and below

H. J. Preston*, L. L. Lim, D. S. Lee and P. D. Hooper
Dalton Research Institute, Department of Environmental and Geographical Sciences, Manchester Metropolitan University, Manchester, United Kingdom

ABSTRACT: The climate change objectives and policies of the European Union are based upon the concept of climate stabilization, with the premise that the climate needs to be stabilized so that temperatures increase by no more than 2°C at 2100. However, the stabilization scenarios currently published do not prescribe where emissions reductions must come from to meet the stabilization of atmospheric CO_2. If the principle of stabilization is to continue to be used as a basis of climate policies, then it will be important to address where the emissions reductions will come from, and to what extent. This paper is a first look at how aviation may or may not be compatible with stabilization. It highlights that aviation emissions have the potential to consume a significant proportion of the emissions budget under stabilization.

Keywords: Aviation, stabilization scenarios, emissions

1 INTRODUCTION

The European Union's (EU's) climate change objectives and policies are based upon the concept of climate stabilization, within which there is the assumption that the climate needs to be stabilized so that temperatures increase by no more than 2°C (CEC, 2007). This paper attempts to determine what fraction of the emissions budget the aviation sector will consume under different growth and technology scenarios for a range of climate stabilization regimes. The aviation industry has until recent years received limited attention regarding its climate impacts, and was not allocated emission targets within the Kyoto Protocol (although it was addressed in Article 2.2 which stated that emissions from aviation and marine bunker fuels should be limited or reduced (UNFCCC, 1998). However, the industry is growing strongly and is projected to do so (projections from aircraft manufacturers predict a doubling of the global civil fleet size from ~20,500 aircraft in 2006 to ~40,500 in 2026 (Airbus, 2007 in Lee *et al*, 2009: 3522)), and whilst currently the climate forcing of the emissions the industry produce are fairly small in global terms (3.5% of total anthropogenic forcing excluding the effects of cirrus clouds), this will increase along with the growth in the industry (Lee *et al*, 2009: 3528). It is evident therefore, that focus on the industry will be important in future climate change policy. Such attention has already become apparent within the UNFCCC draft negotiating text (in preparation for the COP-15 in December), with the acknowledgement that all sectors (including international aviation and shipping) should contribute to limiting emissions (UNFCCC, 2009).

2 STABILIZATION SCENARIOS

Climate stabilization scenarios use an inverse modelling approach which calculates the required emissions and their rate of change, to achieve stabilization of atmospheric CO2 concentrations at different levels (Wigley, 2003). There are a number of climate stabilization scenarios or profiles that have been published, with the first being in 1994 when Working Group 1 (WG1) of the IPCC published a set of stabilization profiles that stabilized atmospheric CO2 concentrations at a variety

* *Corresponding author:* Holly Preston, Centre for Aviation, Transport and the Environment, Manchester Metropolitan University, United Kingdom. Email: h.preston@mmu.ac.uk

of stabilization levels from 750 ppmv to 350 ppmv (IPCC, 1994 in Manne & Richels, 1997: 254). The objective of the profiles was to demonstrate what emissions would be required to reach such stabilization. Following from the WG1 profiles Wigley, Richels and Edmonds developed an alternative set of emissions profiles with the objective of achieving the concentration targets of the WG1 profiles (using the same attainment dates), but by using a different route to stabilization (Wigley et al, 1996). These stabilization scenarios are known as the WRE scenarios. In addition to the WG1 and WRE stabilization scenarios, the Greenhouse Gas Initiative (GGI) has developed another set of scenarios using data derived from the IPCC's SRES scenarios (which have been revised to reflect new information) (IIASA Greenhouse Gas Initiative, 2006). The scenarios include 11 stabilization scenarios for 8 comparable levels, with the lowest stabilization target being 480ppmv. As this paper looks at aviation emissions under stabilization at 450ppmv and below (see Hansen et al, 2008 who posit that a stabilization down to 350 ppm may be more appropriate level to avoid dangerous climate change), the GGI scenarios will not be discussed further.

The emissions and concentration data for the WRE stabilization profiles were taken from MAGICCv5.3 (Model for the Assessment of Greenhouse-gas Induced Climate Change), which is a suite of coupled gas-cycle, climate, and ice-melt models that can determine the changes in the greenhouse gas concentrations, global mean surface temperature and sea level resulting from anthropogenic emissions including CO2, CH4, N2O, VOCs and SO2 (Wigley, 2008). Figure 1shows the CO2 concentration profiles of the WRE stabilization profiles for 650 ppmv down to 350 ppmv. There is a steady increase in CO2 concentrations that then plateau/stabilize at various dates depending on the stabilization target i.e. WRE450 CO2 concentrations stabilize at ~2065, compared with WRE350 CO2 concentrations that stabilize at ~2140.

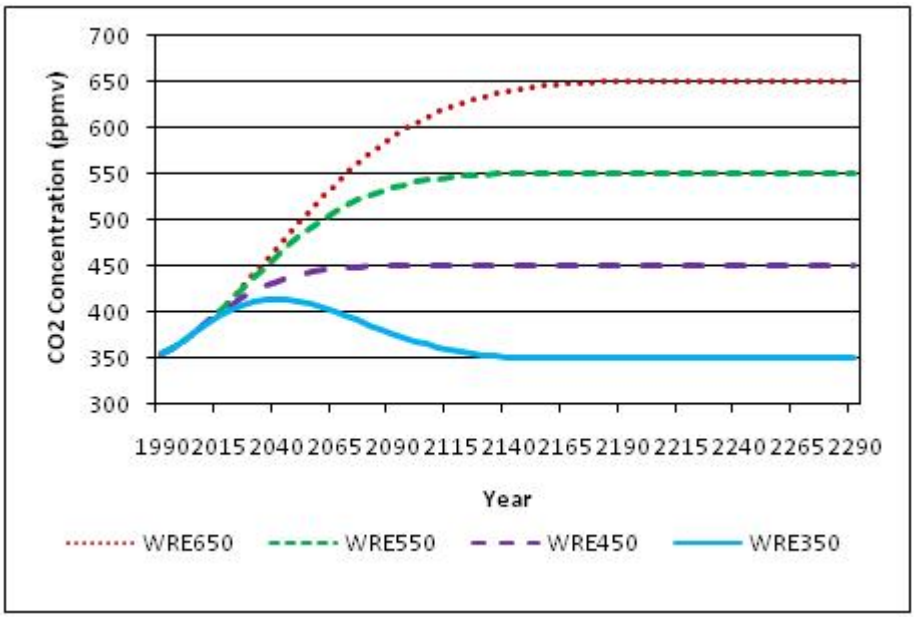

Figure 1. WRE stabilization profiles for CO_2 concentration

The corresponding emissions response for the WRE stabilization profiles are shown in Figure 2, which displays emissions for all scenarios showing a business-as-usual (BAU) pathway that then eventually declines. Again, there are different rates of decline for example, the emissions response under stabilization at 650 ppmv has a longer BAU pathway and a more gradual decline in emissions; compared with the emissions under 350 ppmv which has a very short BAU pathway and then a very rapid decline of emissions, requiring negative emissions at 2065 and then increasing again after 2140. The WRE350 profile has this negative emissions response as that is what would be required to meet the stabilization of atmospheric concentrations of CO_2 at 350 ppmv.

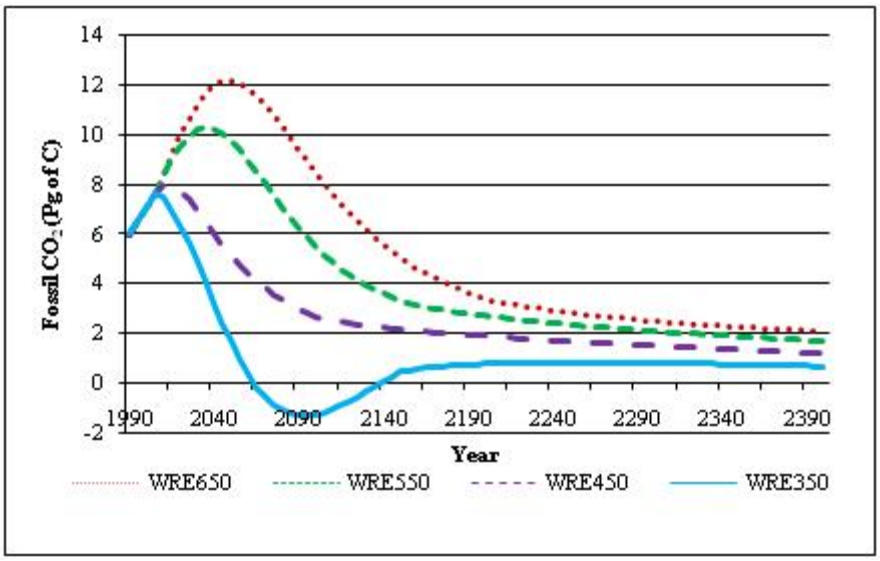

Figure 2. WRE stabilization profiles for emissions response

3 SCENARIOS OF AVIATION EMISSIONS UNDER A CLIMATE STABILIZATION REGIME

The stabilization scenarios do not prescribe from which sectors or sources that the emissions reductions must come from to meet the stabilization of atmospheric CO_2; rather they demonstrate what emissions reductions would be required to do so. If the principle of stabilization is to continue to be used as a basis of climate policies, then it will be important to address where the emissions reductions will come from, and to what extent. This paper aims to look at one part of one sector i.e. aviation emissions.

The aviation emissions data was taken from the European Commission's 6th Framework Project QUANTIFY whereby SRES-based scenarios were developed in a consistent manner for the whole transport sector (Owen & Lee, 2009). Owen and Lee (2009) have created 4 aviation scenarios that follow the assumptions of the SRES A1, A2, B1, B2 storylines. Figure 3 shows the projected aviation emissions for each pathway to 2100.

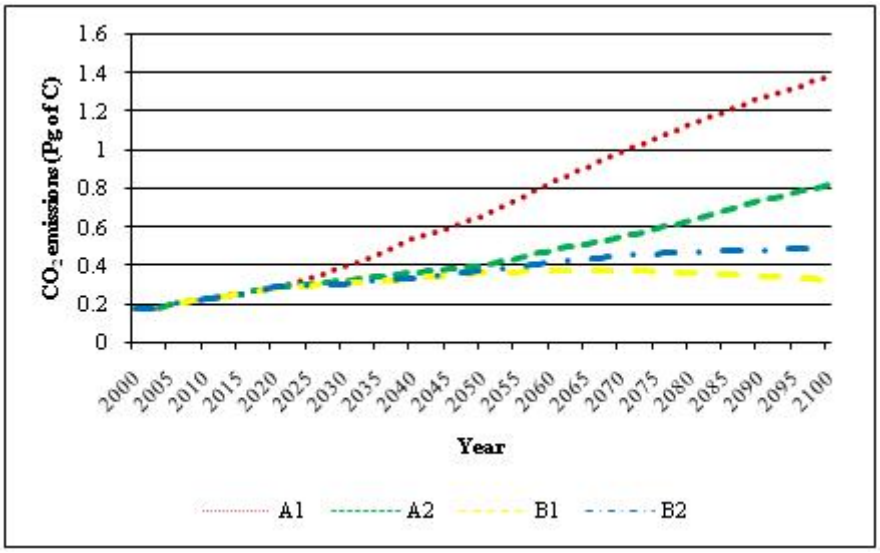

Figure 3. Projected aviation emissions pathway to 2100

Figure 3 shows that the aviation emissions pathways vary considerably depending upon the storyline assumptions. For example, the A1 emissions pathway shows a steady and significant in-

crease in the emissions reaching 1.4 Pg C yr^{-1} by 2100, especially when compared with the emissions pathway under the B1 scenario which only reaches 0.3 Pg C yr^{-1} by 2100. This is consistent with the SRES assumptions as under A1there is an emphasis on very rapid economic growth and the rapid introduction of new technologies; compared with B1in which there is an emphasis on environmental sustainability and the introduction of clean and resource efficient technologies (IPCC, 2000).

To compare the aviation emissions under climate stabilization policies, the CO_2 emissions of the 4 aviation scenarios were plotted with the emissions profiles of the WRE450 and WRE350 stabilization scenarios (see Figure 4). Figure 4 demonstrates that the emissions from the aviation sector will be taking an increasingly significant proportion of the total emissions under stabilization at 450 ppmv, and under 350 ppmv. The outlook is clearly unsustainable, especially under WRE350 where there is the requirement for negative emissions and aviation's emissions are set to continue to increase. Consequently, if aviation emissions were to take the path that the scenarios project, and if climate policies are based on an even more stringent stabilization target than 450 ppmv, then there is a clear incompatibility.

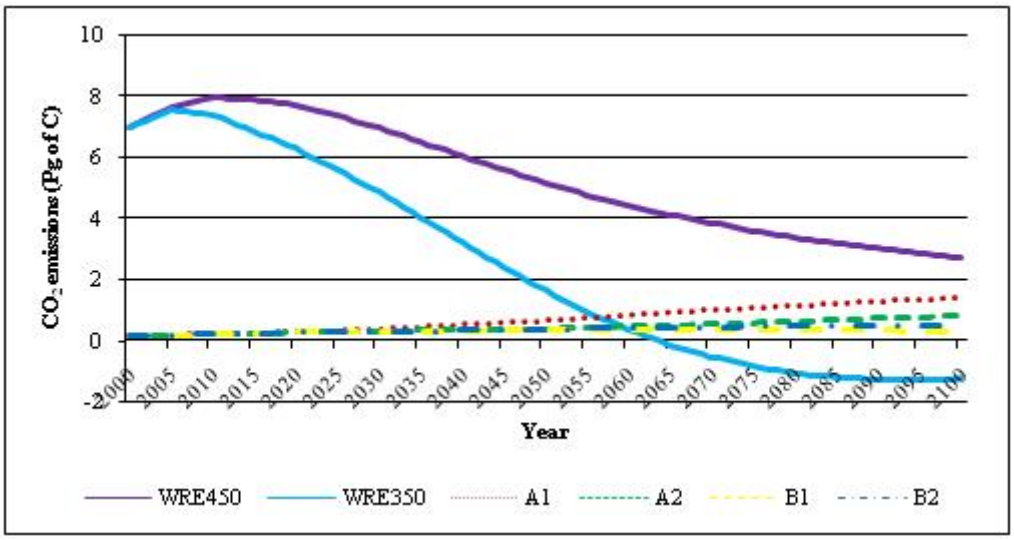

Figure 4. Projected aviation emissions to 2100 compared with WRE stabilization profiles

To demonstrate this further, Figure 5 show the percentage aviation emissions contribution for A1, A2, B1 and B2 scenarios under the WRE450 stabilization scenario (the time-slices for 350 ppmv are not shown due to the fact that after 2055 the aviation sector takes up the entire emissions budget due to the negative emissions scenario).

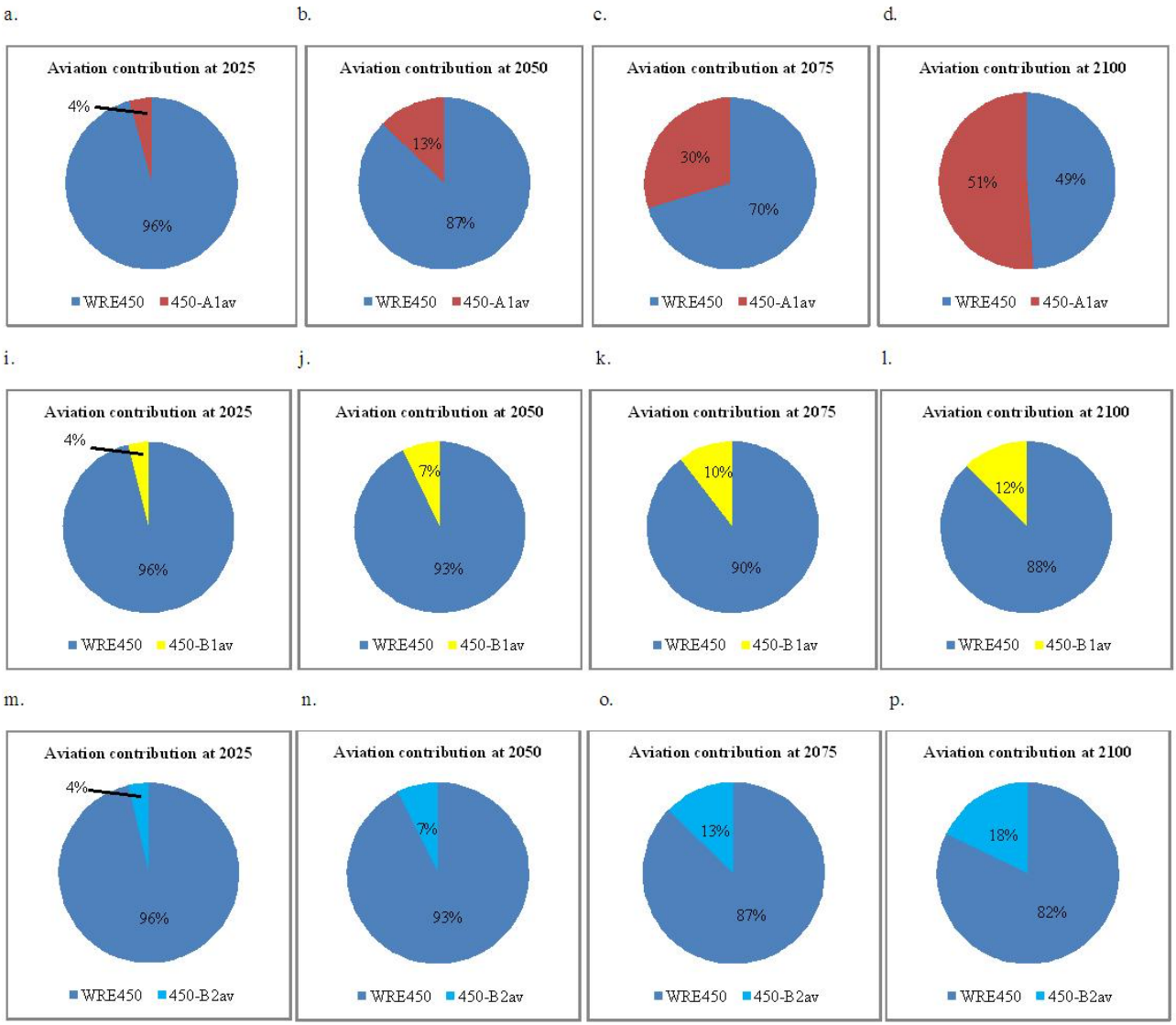

Figure 5. Percentage aviation emissions contribution for 450-A1av, 450-A2av, 450-B1av and 450-B2av scenarios under stabilization at WRE450

The pie charts in Figure 5 show the WRE emissions budget allowable under the WRE450 stabilization scenario for all sectors, with the percentage of the emissions budget that will be consumed by the aviation sector. For example, the time-slices for the 450-A1av scenario (a – d) show that aviation will take up a significantly increasing proportion of the emissions budget allowable under the stabilization regime, and by 2100 over 51% of the emissions budget will be consumed by the sector.

For the 450-B1av scenario (i – l), the percentage of emissions that will be consumed by the aviation sector is considerably smaller, reaching only 12% by 2100. This demonstrates that the feasibility or plausibility of a stabilization regime being successful may depend upon which pathway aviation takes, as some scenarios will be easier to implement when considering all the sectors. For example, under the 450-B1av scenario, there will be a larger proportion of the emissions budget available for other sectors than under the 450-A1av scenario.

4 AVIATION FORCING AND TEMPERATURE RESPONSE UNDER A CLIMATE STABILIZATION REGIME

To determine the forcing and temperature response of aviation CO_2 emissions under climate stabilization at 450 ppmv, the emissions for the 4 scenarios were run in LinClim, a linear climate response model (Lim *et al*, 2007). Figure 6 shows the temperature and response for all 4 scenarios.

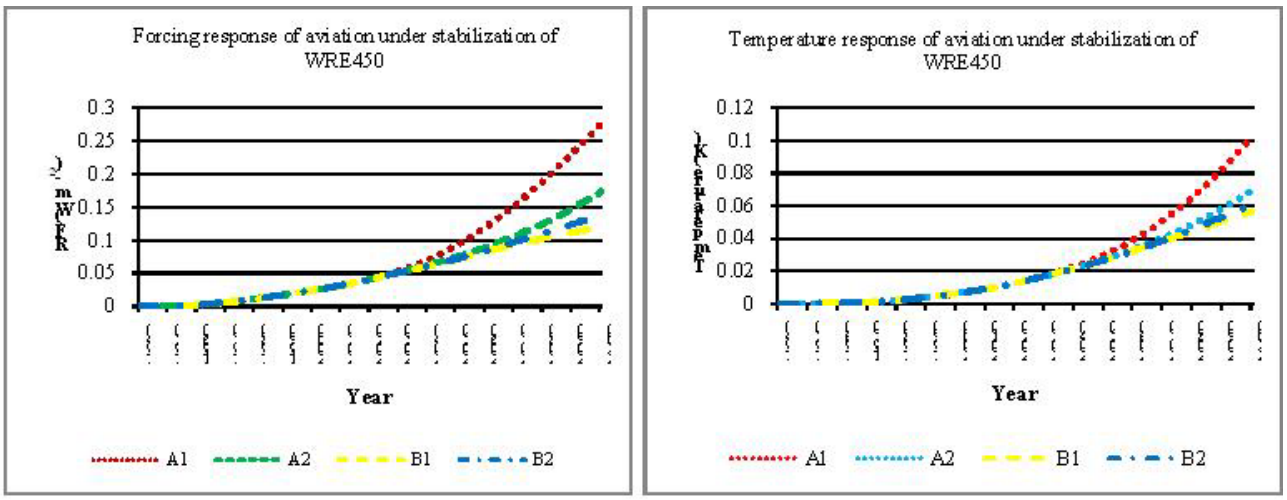

Figure 6. Forcing and temperature response of aviation under climate stabilization of WRE450

The graphs show the varying forcing and temperature response for the 4 aviation scenarios with the A1 scenario having the largest forcing and temperature increase; the temperature increasing by 0.1K in 2100. The B1 scenario has the smallest forcing and temperature response with the temperature increasing by just over 0.6K by 2100. If presented with this information alone, it could be concluded that the climatic impact from the aviation industry's emissions are minimal compared with other sectors. However, it is important to note that these data represent the temperature and forcing for CO_2 alone and aviation has other non-CO_2 RF effects. Therefore, the temperature response for the sector will be greater than the temperature response from just CO_2 alone.

5 DISCUSSION

This paper is a first look at how various aviation scenarios of growth and technological improvement may or may not be compatible with a 450 ppmv stabilization scenario. It is acknowledged that this approach uses a combination of SRES-based scenarios (A1, A2, B1, B2) along with stabilization scenarios, which might be considered to be a mix of inconsistent world outlooks. However the paper serves to illustrate the potential demand for aviation, and what may be required of aviation under policies based upon stabilization.

An important aspect of this paper is to demonstrate the use of modelled data when relating it to specific climate policies. Under EU climate policies, the aim is to reach a stabilization of greenhouse gas emissions so that temperatures do not exceed 2°C. The analysis tells the story of aviation taking an increasing and significant proportion of the emissions allowable under the stabilization profiles, a point which is of use to both the sector and other stakeholders in terms of expectations. Furthermore, the analysis enables a consideration of growth expectations of the sector versus the possibility and feasibility of emissions reductions in other sectors that still allows stabilization at 450 ppmv.

There are a number of questions that this analysis raises. Firstly, if climate policies are to be based upon the principle of climate stabilization, how is this to be achieved and how can the emissions budget be broken down between each of the sectors? One possible solution to this has been presented by Pacala and Socolow with their proposed 'Stabilization Wedges' which divides the emissions reduction budget into 7 equal wedges (representing an emissions reduction action) that could potentially be divided up between sectors or carbon reducing actions (Pacala & Socolow, 2004) e.g. transport sector could be one section/wedge.

Furthermore, as this work has demonstrated, when focusing on just one element of one sector, and only one of the greenhouse gases, under certain future pathways aviation alone has the potential to take up the significant proportion of the emissions budget. What are the potential contributions of the other sectors and the implications that they will have on policy? If this analysis were to be extended further to look at the whole transport sector under stabilization then the complexities of the issue become considerable since, for example, international shipping has similar growth expecta-

tions to 2050 (Buhaug *et al*, 2009). Similarly, policy has mainly focused upon CO_2, if there were to be an emphasis upon the non-CO_2 emissions then again the potential climate impacts of the sector, as well as the uncertainties, are increased.

REFERENCES

Airbus, 2007: Global Market Forecast 2006-2026. Airbus, France.

Buhaug, Ø., Corbett, J.J., Endresen., Eyring, V., Faber, J., Hanayama, S., Lee, D.S., Lee, D., Lindstadt, H., Mjelde, A., Pålsson, C., Wanquing, W., Winebrake, J.J. & Yoshida, K. 2009: *Second Study on Greenhouse Gas Emissions from Ships*, International Maritime Organisation (IMO) London, UK

CEC, 2007: *Communication from the Commission to the Council, The European Parliament, The European Economic and Social Committee, and the Committee of Regions.*

International Institute for Applied System Analysis (IIASA), 2007: *GGI Scenario Database* available online at: http://www.iiasa.ac.at/Research/GGI/DB/

Intergovernmental Panel on Climate Change (IPCC), 2000: *Special Report on Emissions Scenarios* Nakicenovic, N. & Swart, R. (Eds.), Cambridge University Press

Hansen, J., Sato, M., Kharecha, P., Beerling, D., Berner, R., Masson-Delmotte, V., Pagani, M., Raymo, M., Royer, D.L. & Zachos, J.C. 2008: "Target Atmospheric CO_2: Where Should Humanity Aim?, *The Open Atmospheric Science Journal*, 2: 217 - 231

Lee, D.S., Fahey, D.W., Forster, P.M., Newton, P.J., Wit, R.C.N., Lim, L.L., Owen, B. & Sausen, R. 2009: "Aviation and global climate change in the 21st century", *Atmospheric Environment*, 43: 3520 - 3537

Lim, L.L., Lee, D.S., Sausen, R., & Ponater, M., 2007: "Quantifying the effects of aviation on radiative forcing and temperature with a climate response model", In: Sausen, R., Blum, A., Lee, D.S., & Brüning, C. (Eds.) *Proceedings of an International Conference on Transport, Atmosphere and Climate (TAC).* Luxembourg, Office for Official Publications of the European Communities, ISBN 92-79-04583-0, 202-207

Manne, A. & Richels, R. 1997: "On stabilizing CO_2 concentrations – cost-effective emissions reduction strategies", *Environmental Modeling and Assessment 2*: 251 - 265

Owen, B. Lee, D.S. & Lim, L.L. 2009: "Flying into the future – aviation emissions scenarios to 2050". Submitted.

Pacala, S. & Socolow, R. 2004: "Stabilization Wedges: Solving the climate problem for the next 50 years with current technologies", *Science*, 305

United Nations Framework Convention on Climate Change (UNFCCC), 2009: *Ad Hoc Working Group on Long-term Cooperative Action under the Convention*, 6th Session, Bonn 1 – 12 June 2009 Available online at: http://unfccc.int/resource/docs/2009/awglca6/eng/08.pdf

UNFCCC, 1998: *Kyoto Protocol to the United Nations Framework Convention on Climate Change*, available online at: <http://unfccc.int/resource/docs/convkp/kpeng.pdf>

Wigley, T.M.L. 2008: *MAGICC/SCENGEN 5.3: User Manual (Version 2).* Available online at: http://www.cgd.ucar.edu/cas/wigley/magicc

Wigley, T.M. L. 2003: "Modelling climate change under no-policy and policy emissions pathways", *Working Party on Global and Structural Policies. OECD Workshop on the Benefits of Climate Policy: Improving Information for Policy Makers.*

Wigley, T.M.L., Richels, R. & Edmonds, J.A. 1996: "Economics and environmental choices in the stabilization of atmospheric CO_2 concentrations", *Nature* 379: 240 - 243

Global temperature change from the transport sectors: Historical development and future scenarios

R.B. Skeie, J.S. Fuglestvedt *, T. Berntsen, M.T. Lund, G. Myhre, K. Rypdal
CICERO – Center for International Climate and Environmental Research – Oslo, Norway

Keywords: Transport sectors, radiative forcing, temperature, historical emissions, scenarios

ABSTRACT: Transport affects climate directly and indirectly through mechanisms that cause both warming and cooling and operate on very different timescales. In this study, we calculate contributions to the historical development in global mean temperature for the main transport sectors (road transport, aviation, shipping and rail) based on estimates of historical emissions of a suite of gases, aerosols and aerosol precursors, and by applying knowledge about the various forcing mechanisms from detailed studies. Furthermore, we calculate the development in future global mean temperature for four transport scenarios consistent with the IPCC SRES scenarios. We also calculate contributions for a sensitivity test scenario and a mitigation scenario for aviation, which is consistent with the strategic research agenda of the Advisory Council for Aeronautics Research in Europe (ACARE) targets for greening of air transport.
There are large differences between the transport sectors in terms of sign and magnitude of temperature effects and with respect to the contributions from the long- and short-lived components. From pre-industrial times to year 2000, we calculate that transport in total has contributed 9% to a total net man-made warming of 0.76°C. The dominating contributor to warming is CO_2, followed by tropospheric O_3. By sector, road transport is the largest contributor; 11% of the warming in 2000 is due to this sector. Aviation has contributed 4% and rail ~1%. Shipping, on the other hand, has caused a net cooling up to year 2000, with a contribution of -7%, due to the effects of NOx and SO_2 emissions. The total net contribution from the transport sectors to total man-made warming is ~15% in 2050, and reaches 20% in 2100 in the A1 and B1 scenarios. Throughout the 21st century, road transport remains the dominating contributor to warming, followed by aviation. In the aviation mitigation scenario, the temperature increase in 2050 is ~20% less than in the least warming scenario, B1. Due to the anticipated reduction in the sulphur content of fuels, the net effect of shipping switches from cooling to warming by the end of the century. There are significant uncertainties related to the estimates of historical and future net warming, mainly due to aerosol effects, cirrus, contrails and uncertainty in the climate sensitivity.

* *Corresponding author:* Jan S. Fuglestvedt, CICERO, P.O. Box 1129, Blindern, N-0318 Oslo, Norway
Email: j.s.fuglestvedt@cicero.uio.no

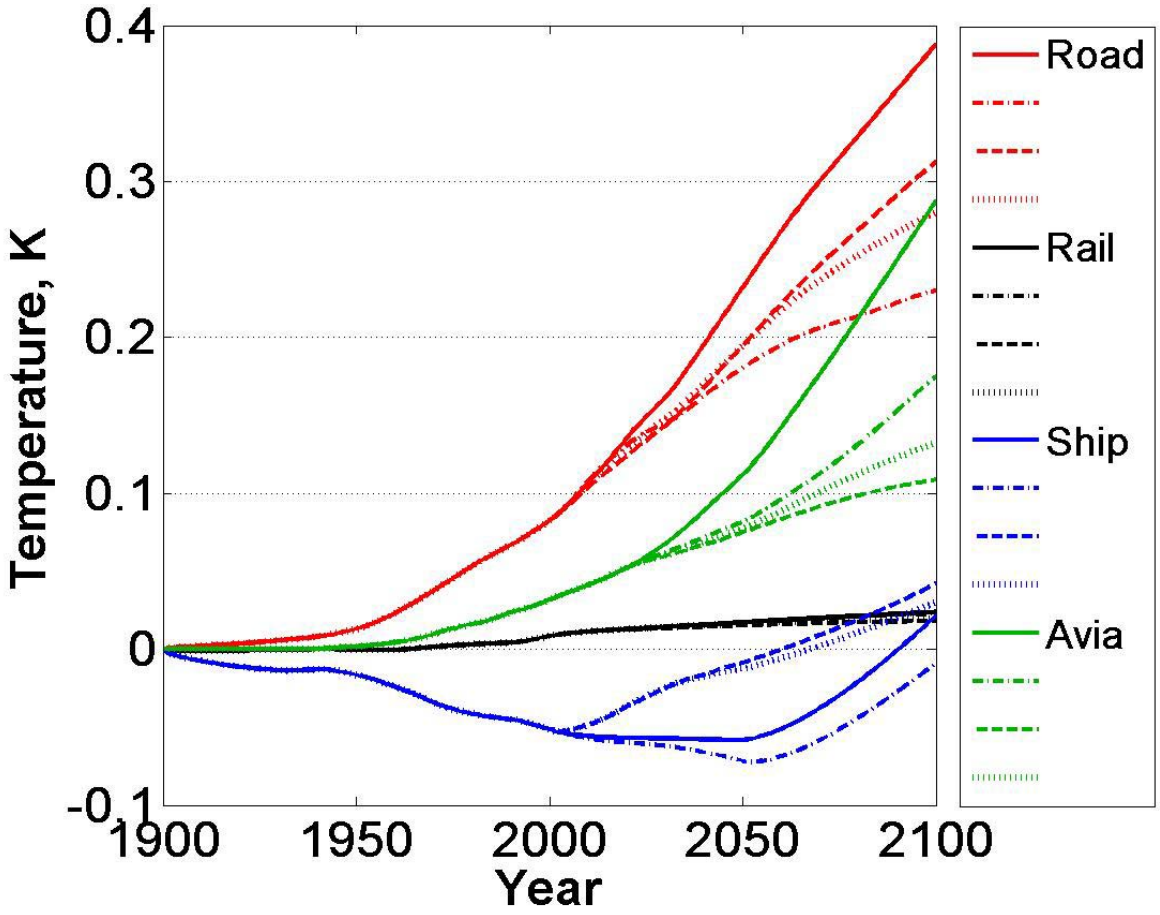

Figure 1. Global mean temperature change due to historical emissions from the transport sectors and future emissions following the four SRES scenarios: A1 (solid), A2 (dash-dot), B1 (dashed) and B2 (dotted).

REFERENCES:

Skeie, R.B., J.S. Fuglestvedt, T. Berntsen, M.T. Lund, G. Myhre, K. Rypdal, 2009: Global temperature change from the transport sectors: Historical development and future scenarios. Atmospheric Environment, in press. http://dx.doi.org/10.1016/j.atmosenv.2009.05.025

Indications of Distinctive Efficacies for Transport Related Ozone Perturbations

M. Ponater *, S. Dietmüller
Deutsches Zentrum für Luft- und Raumfahrt, Institut für Physik der Atmosphäre, Oberpfaffenhofen, Germany

N. Stuber, K.P. Shine, E.J. Highwood, G. Rädel
Department of Meteorology, University of Reading, Reading, UK

Keywords: Ozone, Radiative Forcing, Climate Sensitivity, Efficacy

ABSTRACT: Two series of equilibrium climate change simulations forced by ozone change patterns from transport emissions have been performed with two climate models. It is investigated whether radiative forcings like this lead to climate sensitivity and efficacy parameters that are significantly different among each other and from a reference forcing caused by a homogeneous CO_2 increase. Identification of such differences is complicated by an unexpectedly strong dependence of the climate sensitivity on the strength of certain forcing patterns. Efficacy parameters calculated for the radiative forcings due to ozone increases resulting from aviation, shipping, and land transport emissions vary from unity by no more than 10%. Our results confirm earlier studies that hinted at the necessity to weight radiative forcings from different mechanisms individually in assessment studies, according to their efficacy, but more work is necessary before reliable efficacy parameters can be attributed to such forcings.

1 INTRODUCTION

For a quantitative inter-comparison of climate impact components, metrics of climate change are needed. As discussed by Fuglestvedt et al. (2009), some of these (like radiative forcing) are easy to obtain but difficult to observe in nature, while others (like temperature change) are physically more intuitive but usually hard to determine with the required accuracy. Despite known limitations, the concept of the radiative forcing of climate change has become a standard tool in global climate research (e.g., Shine et al., 1990; Forster et al., 2007) and it is still almost indispensable when small contributions to a total climate effect are to be quantified. However, some implicit basic assumptions have to be re-checked if the concept is applied to new forcing components. Distinctly non-homogeneous forcings have proved to be a conceptual challenge, as model simulations indicate that the fundamental semi-empirical equation linking global surface temperature change (ΔT_{sfc}) to global radiative forcing (RF)

$$\Delta T_{sfc} = \lambda \bullet RF \qquad (1)$$

is often not fulfilled with a universal climate sensitivity parameter λ (e.g., Joshi et al., 2003; Cook and Highwood, 2004; Stuber et al., 2005). Hansen et al. (2005) have pointed out that in cases like this it may still be possible to define a component's (i) climate sensitivity parameter $\lambda^{(i)}$, from which an efficacy factors $r^{(i)} = \lambda^{(i)} / \lambda^{(CO2)}$ can be derived, where $\lambda^{(CO2)}$ indiactes the climate sensitivity of a homogeneous CO_2 increase. This approach would modify Eq. (1) to

$$\Delta T_{sfc} = \lambda^{(i)} \bullet RF = r^{(i)} \bullet \lambda^{(CO2)} \bullet RF \qquad (2),$$

retaining a useful link of ΔTsfc and RF if unique component efficacies $r^{(i)}$ can be determined. Note that both Eq. (1) and (2) imply that the climate sensitivity parameter for all forcings (including CO_2) does not depend on the magnitude of RF, i.e., that ΔT_{sfc} is strictly linear in RF. As shown in Hansen et al. (2005), however, even for CO_2 perturbations moderate deviations from this assumption are

* *Corresponding author:* Michael Ponater, DLR-Institut für Physik der Atmosphäre, Oberpfaffenhofen, D-82230 Wessling, Germany. Email: Michael.ponater@dlr.de

apparent. Hence, in their paper the reference climate sensitivity, $\lambda^{(CO2)}$, has been defined as the climate sensitivity to CO_2 doubling.

Ozone change patterns inferred from precursor emissions of certain transport sectors (aviation, shipping, road traffic) are distinctly non-homogeneous (both horizontally and vertically) and also distinctly different from sector to sector (Hoor et al., 2009). In our study we not only investigated whether different forcing patterns imply the existence of unique efficacies different from unity, but also to which extent the values obtained for $\lambda^{(i)}$ and $r^{(i)}$ are model dependent and method dependent. Moreover, we have checked whether the radiative forcing increases linearly with the amplitude of the ozone change pattern and whether it adds linearly across the sectors

$$RF\ (a \bullet \Delta O3^{(j)}) = a \bullet RF(\Delta O3^{(j)}), \quad RF(\sum \Delta O3^{(j)}) = \sum RF(\Delta O3^{(j)}) \qquad (3a,b),$$

where (j) indicates the three transport sectors mentioned above. Finally, we have also considered whether the temperature response is additive across the sectors:

$$\Delta T_{sfc} = \sum \Delta T_{sfc}^{(j)} \qquad (4)$$

Eq. (4) would be equivalent to requiring that the efficacy parameter of a combination of ozone perturbations can be obtained by linear combination of the respective parameters for individual sectors:

$$r = \sum(RF^{(j)} \bullet r^{(j)}) / \sum RF^{(j)} \qquad (5)$$

We use the ozone change patterns presented by Hoor et al. (2009) as an non-interactive input to two climate models. The respective radiative forcings according to the IPCC are determined. The perturbations are then scaled to ensure statistical significant results for the equilibrium global temperature response and the radiative forcing according to the regression definition (Gregory et al., 2004). The resulting climate sensitivity and efficacy parameters are discussed with respect to their consistency with equations (1) to (5). The reasons for and consequences of deviations from the simple behaviour are suggested.

2 MODELS AND METHODS

Two models have been used for the simulations, viz., ECHAM4/ATT (Stenke et al., 2008) and the UK Met Office Unified Model (UM) (version HADSM3, Williams et al., 2001). Both are full-scale 3-dimensional climate models that are nonetheless economic enough to run many equilibrium climate change simulations including a slab ocean. Each of the runs is at least 45 years long. The first 20 simulation years (spin-up phase) are used to calculate radiative forcings and climate sensitivity parameters (RF_{greg}, λ_{greg}) from the regression method (Gregory et al., 2004). The climate response (e.g., ΔT_{sfc}) is calculated as the difference between the equilibrium states of a climate sensitivity run and a reference simulation. Radiative forcings according to the IPCC definition ('stratosphere adjusted forcing at the tropopause', RF_{adj}) are determined from an extra one-year simulation with the respective radiation code (Morcrette et al., 1986, for ECHAM; Edwards and Slingo, 1996, for UM).

An essential point is the necessity of scaling the original ozone perturbations because, both, the equilibrium temperature response (ΔTsfc) and the parameters derived from the regression method (RFgreg, λ greg) are associated with a statistical uncertainty that renders any simulation with radiative forcing values smaller than about 0.3 W/m2 useless for calculating significant differences between climate sensitivity or efficacy parameters. This emphasizes the crucial role of the linearity assumption for the radiative forcing concept as described in the introduction. ECHAM/ATT as well as the UM have been run with ozone perturbations scaled by factors of 100 and 500. However, for reasons to be explained in section 3 the number of simulations had to be enhanced for ECHAM/ATT.

3 RESULTS

3.1 *Radiative forcing and its linearity*

The results of the radiative forcing calculations for those simulations performed by both models are summarized in Table 1. The RF values based on the regression method (3rd and 5th column) can only be given with sufficient reliability if the perturbations are scaled.

	ECHAM		*UM*	
	RF_{adj}	RF_{greg}	*RF_{adj}*	*RF_{greg}*
CO_2 (doubling)	3.792	3.62	*3.76*	*4.04*
OZavi	0.019	-	*0.015*	-
OZavi (100)	1.593 (82)	1.47	*1.27 (85)*	*1.40*
OZavi (500)	5.730 (295)	5.51	*4.34 (289)*	*4.89*
OZrtr	0.034	-	*0.023*	-
OZrtr (100)	2.646 (77)	2.59	*1.94 (84)*	*2.05*
OZrtr (500)	9.051 (264)	8.32	*6.41 (278)*	*6.70*
OZshi	0.034	-	*0.023*	-
OZshi (100)	2.679 (78)	2.79	*1.93 (84)*	*2.27*
OZshi (500)	9.261 (269)	8.48	*6.36 (276)*	*6.91*
OZsum	0.088	-	*0.061*	-
OZall	0.087 (99%)	-	*0.060 (98%)*	-
OZsum (100)	6.918	6.85	*5.14*	*5.72*
OZall (100)	5.637 (81%)	5.54 (81%)	*4.11 (80%)*	*4.58 (80%)*
	[Wm^{-2}]	[Wm^{-2}]	*[Wm^{-2}]*	*[Wm^{-2}]*

Table 1: Radiative Forcing according to the IPCC definition and according to the regression definition for the scaled ozone perturbations from aviation (avi), road traffic (rtr), and shipping (shi), as calculated with the ECHAM and *UM (marked by italics)* climate models. Values in brackets indicate the enhancement factors for the forcings of the scaled perturbations, or the percentage by which the forcing of the sum of all perturbations [OZall(100)] is reduced compared to the sum of forcings of the individual perturbations [OZsum(100)].

Radiative forcing from CO_2 agrees well between the two models, but ozone forcings are generally larger in ECHAM than in UM. The regression method produces smaller radiative forcings for ECHAM but larger radiative forcings for UM, which may be explained by different feedbacks on the short time-scale (Gregory et al., 2004) for the two participating models. Additivity over the three sectors is almost perfect for the un-scaled ozone perturbations. However, as scaling increases saturation effects show up (particularly in the longwave part of the spectrum), which disturb the linearity in the ozone perturbation/radiative forcing relation. Radiative forcings for the factor 500 scaled patterns exceed the forcing of the un-scaled perturbation only by factors less than 300 in both models. Summarizing, substantial non-linearities in the radiative forcing only occur for excessive scaling.

3.2 *Climate response: model dependence*

Table 2 summarizes, for both participating models, the results of radiative forcing, climate sensitivity, and efficacy as determined using the regression method (RF_{greg}, λ_{greg}, r_{greg}). The reference climate sensitivity for CO_2 doubling is surprisingly similar when compared with model to model differences that have been found elsewhere (e.g., Joshi et al., 2003). However, there is no indication of a universal climate sensitivity parameter for either model. A similar conclusion can be drawn when the values are derived using the IPCC forcings (RF_{adj}, not shown). Moreover, except for the aviation ozone perturbation, the results inhibit a substantial non-linearity of the surface temperature response that is inconsistent with the concept outlined above. For the ECHAM model, in particular, the climate sensitivity and efficacy parameters seem to depend more on the scaling of a pattern than on its spatial structure. A straightforward conclusion about possible efficacy differences for the original (un-scaled) ozone perturbations is thus impossible from the simulations listed in Table 2. Only for aviation ozone these simulations do hint at an efficacy value systematically different from unity; however, in this case ECHAM and UM point in opposite directions, the first model suggesting a higher and the second on a lower efficacy.

	ECHAM				*UM*			
	ΔT_{sfc}	RF_{greg}	λ_{greg}	r_{greg}	*ΔT_{sfc}*	*RF_{greg}*	*λ_{greg}*	*r_{greg}*
CO_2 (doubling)	2.73	3.62	0.78	1	*3.35*	*4.04*	*0.84*	*1*
OZavi (100)	1.17	1.47	0.87	1.11	*0.81*	*1.40*	*0.70*	*0.83*
OZavi (500)	4.83	5.51	0.87	1.11	*3.11*	*4.89*	*0.66*	*0.79*
OZrtr (100)	2.03	2.59	0.81	1.04	*1.60*	*2.05*	*0.86*	*1.02*
OZrtr (500)	8.57	8.32	1.03	1.31	*6.12*	*6.70*	*0.92*	*1.09*
OZshi (100)	1.92	2.79	0.73	0.93	*1.90*	*2.27*	*0.84*	*1.00*
OZshi (500)	8.79	8.48	1.06	1.36	*6.81*	*6.91*	*1.00*	*1.19*
OZall (100)	4.67	5.54	0.87	1.11	*3.53*	*4.58*	*0.82*	*0.97*
OZall (50)	2.52	3.10	0.85	1.09	-	-	-	-
	[K]	[Wm^{-2}]	[K/Wm^{-2}]		*[K]*	*[Wm^{-2}]*	*[K/Wm^{-2}]*	

Table 2: Radiative forcing, climate sensitivity, and efficacy according to the regression definition for the scaled ozone perturbations from aviation (avi), road traffic (rtr), and shipping (shi), calculated with the ECHAM and *UM (marked by italics)* climate models. The surface temperature response (2nd and 6th column) is the true equilibrium climate response and not derived through regression of the spin-up phase of a simulation (see text).

3.3 *Nonlinearities in the forcing-response relationship*

The unexpected and conceptually inconsistent variation of climate sensitivity and efficacy among patterns of the same structure but different scaling has been further explored for the ECHAM model for which this behaviour is most distinct. First, the number of simulations was enhanced to allow a more systematic investigation. Second, we determined the cloud radiative feedback as a likely candidate for the physical origin of the efficacy variations. Analysis confirms this hypothesis (Table 3).

	ΔT_{surf}	RF_{adj}	λ_{adj}	ΔCRF	$\Delta CRF/\Delta T_{surf}$
CO_2 (1 W/m^2)	0.703	1.010	0.696	−0.127	−0.181
CO_2 (doubling)	2.748	3.792	0.724	−0.340	−0.124
CO_2 (tripling)	4.572	6.160	0.742	−0.355	−0.078
OZavi (50)	0.617	0.862	0.716	−0.082	−0.082
OZavi (100)	1.167	1.593	0.733	−0.196	−0.168
OZavi (200)	2.201	2.849	0.773	−0.110	−0.050
OZavi (500)	4.832	5.730	0.843	+0.562	+0.116
OZrtr (100)	2.032	2.646	0.768	−0.034	−0.017
OZrtr (150)	2.900	3.689	0.786	+0.129	+0.044
OZrtr (500)	8.586	9.051	0.949	+3.262	+0.380
OZshi (100)	1.925	2.679	0.719	−0.018	−0.009
OZshi (150)	2.833	3.743	0.757	+0.155	+0.055
OZshi (500)	8.793	9.261	0.949	+3.888	+0.442
OZall (50)	2.524	3.279	0.770	+0.062	+0.025
OZall (100)	4.673	5.637	0.829	+0.774	+0.165
	[K]	[Wm^{-2}]	[K/Wm^{-2}]	[Wm^{-2}]	[Wm^{-2}/K]

Table 3: Equilibrium temperature response, radiative forcing, climate sensitivity, and cloud radiative feedback for ECHAM simulations forced by CO_2 and ozone perturbations (from aviation (avi), road traffic (rtr), and shipping (shi)) with different scaling. Radiative forcing and climate sensitivity are calculated using the IPCC definition (see text). The cloud radiative feedback (ΔCRF) is the equilibrium change of cloud radiative forcing, relative to the reference run.

For all ozone perturbations, increasing scaling induces a gradual change from negative cloud radiative feedback for moderate scaling to ever stronger positive feedback for heavy scaling. This shift to a qualitatively different cloud feedback regime causes higher climate sensitivity in the simulations with heavy scaling of the original perturbation. It is also evident that the shift occurs earlier for shipping than for aviation ozone, suggesting a crucial influence of static stability changes in the lower troposphere and respective consequences for low level clouds. It is notable that the effect of a changing cloud feedback regime is also present, but much less distinct, in case of an increasing CO_2 forcing. Here, the cloud radiative feedback remains negative up to a forcing level of 6 W/m^2, though the specific cloud feedback per unit temperature response (last column in Table 3) slightly decreases. As a consequence, the climate sensitivity increase with an increasing CO_2 forcing remains comparatively moderate and consistent with what is reported by Hansen et al. (2005).

4 NON-LINEAR FIT FOR CLIMATE SENSITIVITY AND EFFICACY

The dependence of the cloud radiative feedback on strength and pattern of the forcing offers a physical explanation for the unexpected increase of climate sensitivity and efficacy with increasing forcing. Assuming the existence of terms of higher order (in RF) in Eq. (1), and requiring that λ approaches a constant value for small radiative forcing, implies that to describe the correlation of climate sensitivity and radiative forcing a parabolic fit (Figure 1) is to be preferred above a linear fit:

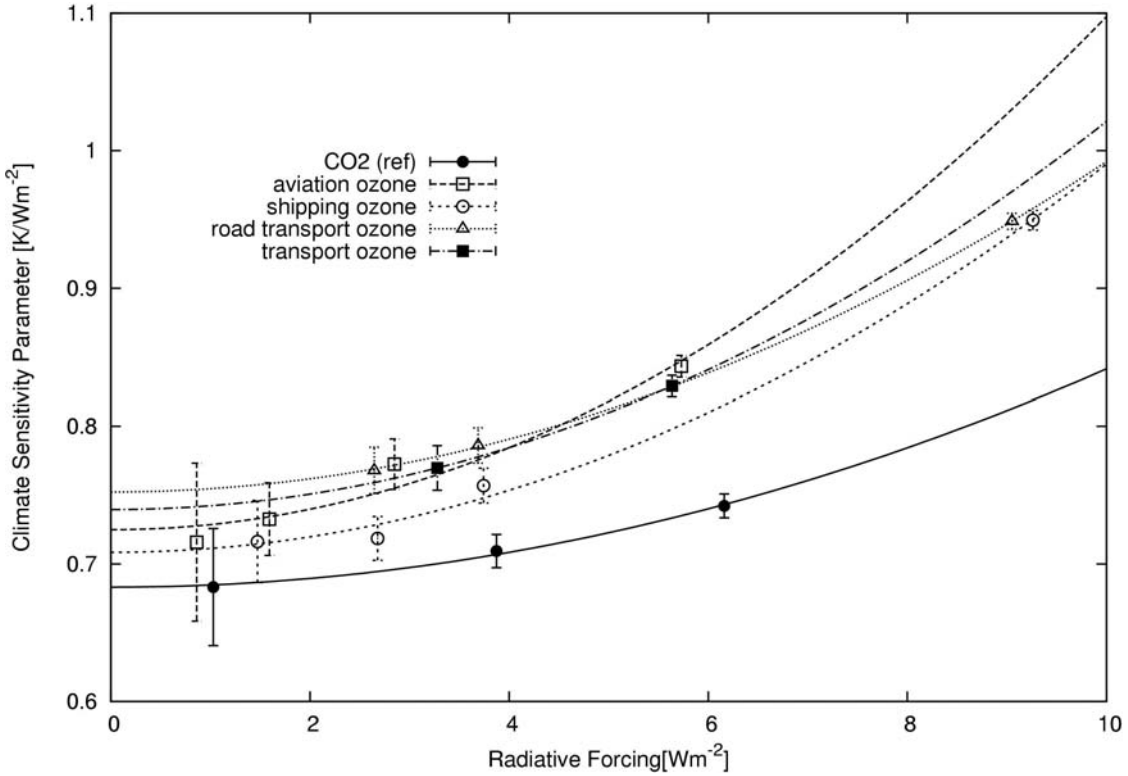

Figure 1: Dependence of the climate sensitivity parameter from the radiative forcing in the series of ECHAM simulations listed in Table 3. The symbols represent the individual simulations for CO2, individual transport sector ozone, and combined transport ozone, respectively. The curves indicate quadratic fits to the individual simulation series. A linear fit is not adopted, in order to ensure that the curves approach horizontal lines as RF approaches zero. The uncertainty bars indicate the 95% confidence interval for the simulated climate sensitivities (which is growing wider as ΔT_{surf} and λ decrease).

By taking the interception of the fitted curves with the ordinate we approximate unique values of the climate sensitivity parameter (λ_{adj}, in this case) for the original (small) perturbations. We apply this definition for all forcings (incl. CO_2), thus diverging from Hansen et al. (2005) who deliberately calculate the efficacy with respect to CO_2 doubling. If we define the efficacy values as explained, all transport ozone efficacies exceed unity and deviate by less than 10%. This means a much smaller excess over unity than found in earlier work (e.g., Stuber et al., 2005), probably because the perturbation patterns used here are smoother compared to the idealized patterns used in previous studies.

	λ_{adj}	r_{adj}
CO_2	0.692	1
OZavi	0.725	1.048
OZrtr	0.752	1.088
OZshi	0.707	1.021
OZall	0.739	1.068
OZall (approx)	0.729	1.053
	[K/Wm^{-2}]	

Table 4: Climate sensitivity and efficacy parameters derived from the parabolic fit of the results from the ECHAM simulations with individual transport related ozone perturbation patterns. The last line includes values of the same parameters derived for transport ozone by linear combination of the RF weighted values from the individual sector contributions.

Table 4 summarizes the respective values for λ_{adj} and r_{adj} reached in this way. It is suggested that, qualitatively, the ozone change pattern from road traffic has the largest efficacy while shipping ozone has the lowest efficacy close to unity. Using equation (5) to calculate a combined efficacy for a simultaneous forcing involving all transport sectors (OZall(approx)) yields satisfactory agreement with the fitted efficacy from dedicated runs with the same combination of forcings (OZall).

5 CONCLUSIONS AND OUTLOOK

Results from two series of equilibrium climate change simulations with respect to ozone perturbations caused by emissions by the transport sector confirm earlier findings suggesting the existence of efficacies significantly deviating from unity for this kind of non-homogeneous radiative forcing. Differences from the reference case (homogeneous CO_2 increase) are, however, not as large as found in previous studies which used idealized perturbation patterns. Individual ozone patterns clearly tend to show up distinctive efficacy values but inter-model differences render quantitative conclusions only indicative. A strong dependence of the climate sensitivity on the strength of a radiative forcing has become obvious from the simulations analysed for this study; this has required an extra effort to quantify well-defined efficacy value for some of the perturbation patterns.

In view of the difficulties in determining method-independent efficacy values, the relatively small deviation of the efficacies of transport related ozone perturbations from unity (not larger than 10 %), and occasional qualitative contradictions between the results of the two participating climate models, care is required when introducing the efficacy values from our simulations in assessment studies (e.g., Fuglestvedt et al., 2008). They may be used to test how sensitive a comparison of transport sector climate impacts depends on including distinctive efficacies. A more comprehensive understanding, validation of key feedbacks, and a consensus between different climate models will be necessary, however, before we can claim for sure that climate impact assessments are improved by the use of distinctive efficacies.

6 ACKNOWLEDGEMENTS:

The QUANTIFY project is funded by the European Union within the 6th Framework Project under contract 003893.

REFERENCES

Cook, J. and E.J. Highwood, 2004: Climate response to tropospheric absorbing aerosols in an intermediate general-circulation model. Q. J. R. Meteorol. Soc. 130, 175-191.

Edwards, J.M., and A. Slingo, 1996: Studies with a flexible new radiation code. I: Choosing a configuration for a large scale model. Q. J. R. Meteorol. Soc., 122, 689-719.

Forster, P., et al., 2007: Changes in atmospheric constituents and in radiative forcing. In: Climate change 2007: The physical science basis. Contribution of Working Group I to the 4th assessment report of the IPCC (Eds.: Solomon, S., et al.), Cambridge Univ. Press, Cambridge, UK and New York, NY, USA.

Fuglestvedt, J., T. Berntsen, G. Myhre, K. Rypdal, and R. B. Skeie, 2008: Climate forcing from the transport sectors, PNAS 105, 454-458, doi:10.1073/pnas.0702958104.

Fuglestvedt, J., K.P. Shine, T. Berntsen, J. Cook, D.S. Lee, A. Stenke, R.B. Skeie, G.J.M. Velders, and I.A. Waitz, 2009: Transport impacts on atmosphere and climate: Metrics, Atmos. Environ., in press, doi: 10.1016/j.atmosenv.2009.04.044.

Gregory, J., et al., 2004: A new method diagnosing radiative forcing and climate sensitivity. Geophys. Res. Lett. 31, L03205, doi:10.1029/2003GL018747.

Hansen, J., M. Sato, R. Ruedy, L. Nazarenko, A. Lacis, G.A. Schmidt, G. Russell, et al., 2005: Efficacy of climate forcings. J. Geophys. Res. 110, D18104, doi: 10.1029/2005GL022740.

Hoor P., et al., 2009: The impact of traffic emissions on atmospheric ozone and OH: results from QUANTIFY. Atmos. Chem. Phys. 8, 3113-3136.

Joshi, M.M., K.P. Shine, M. Ponater, N. Stuber, R. Sausen, and L. Li, 2003: A comparison of climate response to different radiative forcings in three general circulation models: towards an improved metric of climate change. Clim. Dyn. 20, 843-854, doi: 10.1007/s00382-003-0305-9.

Morcrette, J.-J., L. Smith., and Y. Fouquart, 1986: Pressure and temperature dependence of the absorption in longwave radiation parameterizations. Beitr. Phys. Atmos., 59, 455-469.

Shine, K.P., et al., 1990: Radiative forcing of climate. In: Climate change: The IPCC scientific assessment (Eds.: Houghton, J.T., et al.), Cambridge University Press, Cambridge, New York, Melbourne, Sydney.

Stenke, A., V. Grewe, V., M. Ponater, 2008: Lagrangian transport of water vapour and cloud water in the ECHAM4 GCM and impact on the cold bias. Clim. Dyn., 31, 491-506, doi: 10.1007/s00382-007-0347-5.

Stuber, N., M. Ponater, and R. Sausen, 2005: Why radiative forcing might fail as a predictor of climate change. Clim. Dyn. 24, 497-510, doi:10-1007/s00382-004-0497-7.

Williams, K.D., C.A. Senior, and J.F.B. Mitchell, 2001: Transient climate change in the Hadley Centre models: The role of physical processes. J. Clim., 14, 2659-2674.